American Journal of Chemistry 2022, 12(2): 23-31
DOI: 10.5923/j.chemistry.20221202.01

Synthesis of Iron Nanoparticles from Acid Mine Drainage Using Hydrazine as Reductant

Alegbe M. J.[1,2,*], Moronkola BA[1], Osundiya M. O.[1], Adekolurejo E.[3], Ajewole B. S.[1], Petrik L. F.[2]

[1]Chemistry Department, Lagos State University, LASU Post office, Ojo, Lagos Badagry-Expressway, Lagos, Nigeria
[2]Enviromental and NanoSciences Group, Chemistry Department, University of the Western Cape, Bellville, South Africa
[3]Ogun State Institute of Technology, Igbesa, Ogun State, Nigeria

Abstract Iron-rich acid mine drainage (AMD) is a toxic wastewater generated from the oxidation of pyritic metal ores with water and oxygen to form coloured liquid solution and the disposal of the wastewater becomes a nuisance to the environment. The aim of this study is to use commercial reagent grade and iron-rich AMD solution as a ferric iron source to synthesize iron nanoparticles. Chemical precipitation reduction method was used to synthesize the iron nanoparticles using hydrazine as reductant. The solid residues obtained from the synthesis were characterized using analytical techniques such as inductively coupling plasma-optical emission spectroscopy (ICP-OES), ion chromatography (IC), X-ray diffraction (XRD), scanning electron microscopy (SEM), High resolution transmission electron microscopy (HRTEM), X-ray fluorescence (XRF), and Brunuaver-Emmett Teller (BET). The results of the XRD analysis identified Goethite and magnetite mineral phases for AMD and commercial reagent grade ferric sources respectively. The SEM images of the two iron nanoparticles revealed spherical morphology. The HRTEM analysis revealed a tiny spherical particle structure with average particle size of 4.95 ± 0.55 nm and 8.66 ± 0.58 nm for reagent grade and AMD ferric iron sources respectively and the XRF analysis result revealed that the samples are very rich in Fe iron but reagent grade is richer than the AMD ferric iron source. In conclusion, iron-rich acid mine drainage waste solution was used as a source of ferric salt for the synthesis of quality iron nanoparticles using hydrazine.

Keywords Iron nanoparticles, Acid mine drainage, Reductant, Chemical precipitation, Characterization

1. Introduction

Iron nanoparticles is one the novel nanomaterials that is synthesized and could be applied in different fields because of its distinct properties [1]. With the aid of nanotechnology, bulk material can be manipulated to make them stronger, lighter, durable, extremely reactive and conductive materials. The positive impact of nanotechnology is that, it is a fast growing technology because of its remarkable potential and application of manipulating bulky materials to a nanoscale [2]. The fabrication of zerovalent iron nanoparticle is very important because of its potential in wastewater treatment process and other applications [3]. Iron nanoparticles (INPs) have been found to be very effective in so many applications and it can be used for the removal of contaminant because they are very reactive and possesses high surface area [4]. The synthesis of iron nanoparticles depends on the purity of the reagent used, speed, concentration of solution, temperature, time, etc. Iron nanoparticles can be classified into three categories which are: (i) iron oxide nanoparticles (IONs) consist of magnetite (Fe_3O_4), maghemite (γFe_2O_3), hematite (αFe_2O_3); (ii) iron oxide hydroxide (FeOOH) nanoparticles and (iii) zero-valent iron (ZVI) nanoparticles [5]. Nanomaterials exhibit electrical, optical, magnetic, chemical, and some related surface properties that are entirely different from their respective bulk materials [6]. Synthesis of iron nanoparticles can be top-down or bottom-up approach but the top-down approach involves breaking down of large solid substance to nano-sized particles by different technological routes/methods while the bottom-up grow nanostructured materials [7]. Recently, focus has been on the synthesis of different types of iron nanoparticles as medical nanomaterials. Synthesis of iron nanoparticles by reduction method has a long time history dated as far back in the seventies and eighties [8]. The physical methods used in the synthesis of magnetic iron nanoparticles are milling [9], etching or machining [10], [11], [12] [13] and the chemical methods are: precipitation [14], [15], [16], hydrothermal [17], sonochemical [18], [19], thermal decomposition [20], ultrasonication [21], [22], [23], solvothermal [24], [25], etc. The precipitated iron nanoparticles are characterized with small particle sizes, large surface area and high reactivity. The morphology of the iron nanoparticles can be controlled by the flow rate of reductant solution, pH, and temperature of the reaction

* Corresponding author:
alegbemj@gmail.com (Alegbe M. J.)
Received: Jan. 31, 2022; Accepted: Feb. 28, 2022; Published: Mar. 24, 2022
Published online at http://journal.sapub.org/chemistry

condition [26]. The purpose of this study is to synthesize magnetic iron nanoparticles from iron-rich acid mine drainage (AMD) waste solution using hydrazine as reductant, the iron-rich AMD which could serve as an alternative or substitute to commercial reagent grade ferric chlorides/ferric sulphates salts and to assess the quality of the synthesize iron nanoparticles.

2. Experimental

2.1. Sample Collection

Raw acid mine drainage (RAMD) water samples collected from navigation coal mining site in Mpumalanga province of the Republic of South Africa were collected in 5L plastic containers and stored in the refrigerator at a temperature of 4℃. The AMD samples were filtered with 0.45 µm membrane filter to remove particulate materials present. Nitrogen gas was bubbled into the deionized water so as to de-oxygenate for about 30 minutes before use. All chemicals used without further treatment or purification include absolute alcohol, hydrazine are reagent grade purchased from Merck chemicals.

2.2. Synthesis

(**A**) 200 mL iron-rich AMD sample collected from Navigation coal mine was measured into a 500 mL beaker and subjected to continuous stirring with magnetic stirrer. A 50 mL of 0.9 M hydrazine solution was added to the iron-rich sample and stir constantly with magnetic stirrer for adequate mixing of the mixtures at a temperature of 70℃. A brownish yellow precipitate was formed with a gradual change of colour of the solution from yellow to colourless. The precipitate in the mixture solution was filtered with a 0.45 µm membrane filter. The precipitate was washed with 100 mL ultrapure water twice before drying with nitrogen gas. The residue was dried and weighed continuously until a constant mass was obtained. The dried residue was kept in a sample container and characterized using XRD, HRSEM, HRTEM, XRF, BET and FTIR.

$$4Fe^{3+}\,(aq) + 3N_2H_4\,(aq) + 6H^+\,(aq) + 6H_2O\,(aq) \longrightarrow 4Fe^{0} + 6NH_4OH\,(aq) \quad (1)$$

(**B**) Ferric chloride hexahydrate ($FeCl_3{\cdot}6H_2O$, 98%) was purchased from Merck and used without further purification. 0.1 M of reagent-grade ferric chloride solution was prepared in which 100 mL of the solution was measured into a 250 mL beaker and saturated with nitrogen gas for 30 minutes and stirred constantly. 50 mL of 0.5M N_2H_4 solution was added gradually into the ferric chloride solution with constant stirring at 70℃ a black precipitate was obtained. The black particles precipitated was separated with a strong magnet before washing with 100 mL of deionized water twice and 100 mL absolute alcohol once and immediately sonicated for 10 – 15 minutes to make the particles to be well dispersed. The precipitate obtained was dried with nitrogen gas and weighed until a constant weight was obtained before recording the weight.

$$4Fe^{3+}\,(aq) + 3N_2H_4\,(aq) + 6H^+\,(aq) + 6H_2O\,(aq) \longrightarrow 4Fe^{0} + 6NH_4OH\,(aq) \quad (2)$$

2.3. Characterization

The chemical composition of the iron-rich AMD was determined with Varian Radial Inductively Coupled Plasma Optical Emission Spectroscopy (ICP-OES) and a Dionex DX-120 Ion Chromatography with AS40 automated sampler, ASRS-300 suppresser, AS14 analytical column, AG14guard column and a detector was used for the analysis. The iron oxide phase in the black and orange powdered particles were separately identified with an x-ray powder diffraction patterns using on a Bruker D8 Advance x-ray diffractometer with Cu Kα radiation (45kV, 40mA, λ = 1.542Å). Scan was conducted from 10° to 80° (2θ). The morphology and particle size of synthesized iron nanoparticles were examined with both scanning electron microscopy (SEM) and transmission electron microscopy (TEM). Dried iron nanoparticle samples placed on the coated carbon grid was allowed to dry at room temperature before the SEM analysis was conducted using a HITACHI S-4700 electron microscope. Morphological analysis was carried out using Phillips Tecnai F20 super-twain TEM and the iron nanoparticle was prepared by putting little amount of the particles in a sample bottle containing 5ml absolute alcohol and sonicated for 10 minutes to obtain a good particle dispersal on the copper grid and allowed to dry at room temperature. TEM analysis was carried out to was examined the size and morphology of the iron nanoparticle samples. Surface areas (BET area) of the iron nanoparticle samples obtained from different sources were measured at a temperature of 77.35 K using nitrogen adsorption method with a quantachrome NOVA 2000 surface analyzer. Before the BET analysis, the samples were prepared by washing the iron nanoparticles with acetone and drying them at 100℃ for 5-8 hours under the flow of nitrogen. Only a small amount of the sample was required for the analysis by FTIR. The FTIR instrument was first cleaned and then it was set-up to obtain a background spectrum trial before the sample analysis. A small quantity of the test sample powder was placed on the sample holder of the attenuated total reflectance (ATR) attachment where a specified force was applied for analysis. The instrument produced a spectrogram of the test sample, which gives a reflection of sample quality through their peaks of absorbance or transmittance. Vibrations of some of the functional groups common to the analyzed samples were identified and used for resolution of molecular structures of compounds. Small amount of the iron sample was required for the FTIR analysis. The sample powder was dried in an oven regulated at 105℃ for 12 hours to remove any trace of moisture present in the synthesized iron. The FTIR instrument was first cleaned and then set-up to obtain a background spectrum trial before the sample analysis. A small quantity of the test sample powder was placed on the sample holder of the attenuated total reflectance (ATR)

attachment where a specified force was applied for analysis. The instrument produced a spectrogram of the test sample, which gives a reflection of sample quality through their peaks of absorbance or transmittance. Vibrations of some of the functional groups common to the analyzed iron samples were identified and used for resolution of molecular structures of compounds. Atomic force microscope (AFM, Veeco, Nanoscope IV Digital Instruments) was used to characterize the size and morphology of the synthesized iron nanoparticles.

3. Results

3.1. Chemical Composition of AMD

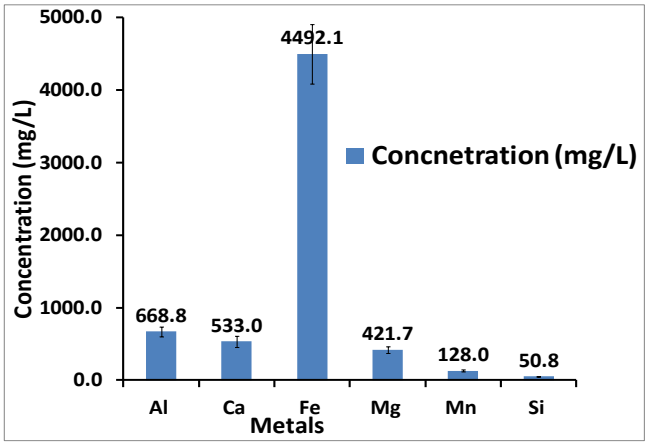

Figure 1. ICP concentration (mg/L) of major species in AMD. Experimental conditions: concentration of AMD = 4492.1 mg/L, pH = 2.14, EC = 7.16 and TDS = 5.94, n = 3

The analysis of the raw AMD sample revealed that it was characterized with low pH (2.14), high electrical conductivity (7.16 mS/cm) and high total dissolved solids (5.94 mg/L). The chemical composition of raw AMD was conducted with inductively coupled plasma optical emission spectroscopy (ICP-OES) and it showed that the sample consist majorly of dissolved metals such as iron, calcium, magnesium, aluminum, silicon, and manganese in high concentration. From the analysis the mine water, the AMD was found to be very rich in ferrous and ferric iron metals (3492.33 mg/L) which could be due to the geological composition of the site and the amount of oxygen available for the oxidation of rock metal tailings. Figure 1 revealed that iron has the highest concentration of some of the dissolved metals present in the raw AMD which implies that the iron-rich AMD would be a good source of iron as raw material for making iron nanoparticles. The AMD analysis revealed 62.96% Fe content which indicated Fe to be the predominant and most abundant metal with the highest concentration (4492.1 mg/L) while the other metal compositions are Al (668.8 mg/L), Ca (533.0 mg/L), Mg (421.7 mg/L), Mn (128.1 mg/L), Si (50.8 mg/L). Other metals are present in the AMD were very low in concentration. The concentration of anions present in the mg/L, AMD solution revealed the concentrations of NO_3^-, Cl^-, and SO_4^{2-} are 56.72 mg/L, ND and 22,587 mg/L respectively.

3.2. XRD

Figure 2 is the XRD spectra of synthesized iron nanoparticles HAI (A) and HFCI (B) using JCPDS database at reflection angles where characteristic peaks of a particular mineral phase can be seen on the spectrum. The diffraction pattern of peaks exhibited by the synthesized nanoparticle HAI (A) whose reflection angles are indexed at 21.88°, 26.46°, 33.85°, 47.79°, 54.2°, 63.38°, 65.84°, 71.12° and 79.12° corresponds to goethite mineral phase. This diffraction pattern can be indexed to goethite [α-FeO(OH)] mineral phase and the assignment of these peaks agrees with some previously reported studies in the literature [27], [16], [22], [23], [28] and the peaks that are slightly broadened indicate that the iron nanoparticles have smaller crystal size [29]. The diffraction peak at reflection angle indexed at 45.3° corresponded to pure iron (α-Fe) mineral phase which indicate the presence of zerovalent iron (α-Fe) with some amorphous crystallinity [30], [31]. The XRD pattern of synthesized HCFI (B) nanoparticles presented in Figure 2, identified a characteristic pattern of magnetite (Fe_3O_4) mineral phase. Twelve major peaks of 2θ angle reflection indexed at 18.3°, 30.1°, 35.3°, 43.1°, 53.3°, 57.1°, 62.5°, 70.94°, 73.9°, 74.48°, 78.32° and 86.71° corresponds to diffraction at (111), (220), (311), (400), (422), (333), (440), (620), (533), (622), (444) and (642) lattice planes, respectively. JCPDS 19-0629 correspond to cubic magnetite mineral phase and the peak at reflection angle at 35.3° of the HFCI (A) nanoparticles corresponds to spinel phase of magnetite (Fe_3O_4). The peaks of HFCI (B) nanoparticles showed no unassigned peaks which means that the sample was a pure and crystalline magnetite mineral phase. The black colour of the powder was further verified that the sample was magnetite mineral phase. The peak broadening of the XRD patterns indicates the small size of the synthesized particles. The XRD result of HFCI particle is consistent with those reported in previous studies [32], [33]. The mineral phases of the HAI (A) and HFCI (B) nanoparticles were both crystalline in nature. The crystallinity and crystal phases of the HAI (A) and HFCI (B) were examined by X-ray diffraction (XRD) in Figure 2 and the results revealed several well defined diffraction reflection peaks which are seen in the observed XRD pattern which matched with the face-centred cubic structures with calculated lattice constants of a = 8.39700 Å . The observed XRD pattern is well matched with previously reported literature [34]. JCPDS card no. 01-082-1533 face centred cubic with no reflection for other impurities was found in the pattern of HFCI (B) which reveals that the prepared nanoparticles are pure synthesized magnetite. But HAI (A) nanoparticles exhibited a trace peak of pure iron at reflection angle 45.3°. However, with the sharp and strong diffraction reflection peaks, one can say that the HFCI (B) is more

crystalline than HAI (A) nanoparticles. The average particle size was calculated by Debye Scherrer formula: $D = 0.9\lambda/\beta\cos\theta$ Where, D is thickness of nanoparticle, λ is wavelength of X-ray, β is half maxima of reflection at bragg's angle 2θ and θ is diffraction angle or bragg's angle.

3.3. SEM-EDS

Figure 3 presents SEM-EDS of the synthesized iron nanoparticles HAI (A) and HFCI (B) gave morphology that appear as tiny strand-like structures called nanowires with particle size range from 48-105 nm. The bare nanowire morphology of HAI (A) synthesized from iron-rich AMD looks like that of HFCI (B) which has been reported in the literature [35], [36]. The EDS spectral analysis of HAI (A-1) and HFCI (B-1) in Figure 3 revealed the type of elements present in the HAI (A) which are O, Fe Al, and S while HFCI (B) are O and Fe only. The presence of Al and S in the HAI can be attributed to the presence of Al and SO_4 in the iron-rich AMD sample are some of the components of the AMD identified from ICP-OES and IC analysis respectively. Table 1 presents the EDS elemental composition of HAI and HFCI nanoparticles. The SEM-EDS elemental composition result of the iron nanoparticles presented in Table 1, revealed the Fe composition of HAI and HFCI as 70.08 ± 3.96% and 75.8 ± 5.85% respectively. The elemental compositions of HAI and HFCI nanoparticles are Al, O, S, and Fe. The HAI is composed of O (20.64%), S (8.26%), Al (1.66%) and Fe (70.08%) while the HFCI is composed of O (24.11%), and Fe (75.8%) elements. This implies that Fe constitute bulk of the particles formed from the reduction process. However, the composition of Fe present in the HFCI nanoparticle is slightly higher than that of HAI but the EDS is only a qualitative technique and not quantitative. It gives accurate information of the type of elements present in a sample but not the accurate quantities of the elements. The iron nanoparticles made from acid mine water revealed that the AMD contained iron sulphate salt while the commercial iron chloride salt contained iron chloride. The presence of Al, and S in the HAI can be attributed to the presence of Al and SO_4 in the iron-rich AMD sample identified from ICP-OES and IC analysis respectively.

Table 1. EDS elemental composition of HAI and HFCI nanoparticles. Experimental condition: AMD pH = 2.14, $FeCl_3$ pH = 1.63, temp = 70℃, speed = 250 rpm, vol. of AMD = 100 mL, vol. of N_2H_4 = 50 mL, Conc. of N_2H_4 = 0.9 M, time = 60 mins and n = 3, HAI = Hydrazine AMD synthesized iron, HFCI = Hydrazine ferric chloride synthesized iron

ELEMENTS	HAI (% atomic wt)	HFCI (% atomic wt)
Fe	70.08 ± 5.85	75.8 ± 3.96
O	20.04 ± 0.6	24.11 ± 1.38
S	8.26 ± 0.03	ND
Al	1.66 ± 0.01	ND

ND = Not detected

3.4. HRTEM

The HRTEM of synthesized iron nanoparticles HAI (A) and HFCI (B) presented in Figure 4 shows that the iron particles are spherical in shape and monodispersed with particle sizes determined using ImageJ software. The crystal size distribution of synthesized iron nanoparticles HAI (A) and HFCI (B) shows that the crystal distribution of the iron particles have average crystal size statistically calculated values of 8.66 ± 0.55 nm and 4.95 ± 0.58 nm for HAI and HFCI respectively. The HRTEM images revealed that these iron nanoparticles are single crystalline as shown by the atomic lattice fringes [9]. The ring-type pattern of the selected area electron diffraction (SAED) analysis for the two particles shows that the monodispersed iron particles were crystalline with their rings. The result shows that the crystal size of the HFCI (B) had smaller particle size than HAI (A). The particle average diameter can be calculated using Scherrer's formula. The average calculated particle sizes for HAI and HFCI in Figure 2 were about 9.81 ± 0.43 nm and 5.37 ± 0.31, which are close to the 8.66 nm and 4.95 nm average particle sizes determined by statistical analysis of the TEM images for HAI and HFCI respectively.

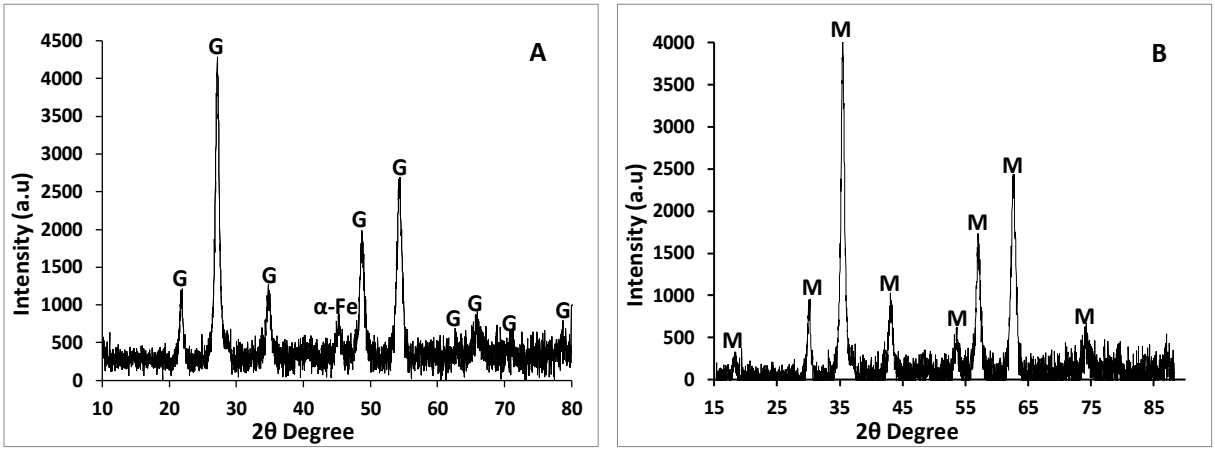

Figure 2. XRD analysis of synthesized iron from HAI (A) and HFCI (B) nanoparticles. Experimental conditions: pH = 2.14, $FeCl_3$ pH = 1.63, temp = 70℃, speed = 250 rpm, vol. of AMD = 100 mL, vol. of N_2H_4 = 50 mL, Conc. of N_2H_4 = 0.9 M, time = 60 mins and n = 3. G = goethite, M = magnetite, HAI = Hydrazine AMD iron, n = 3, HAI = Hydrazine AMD synthesized iron, HFCI = Hydrazine ferric chloride synthesized iron

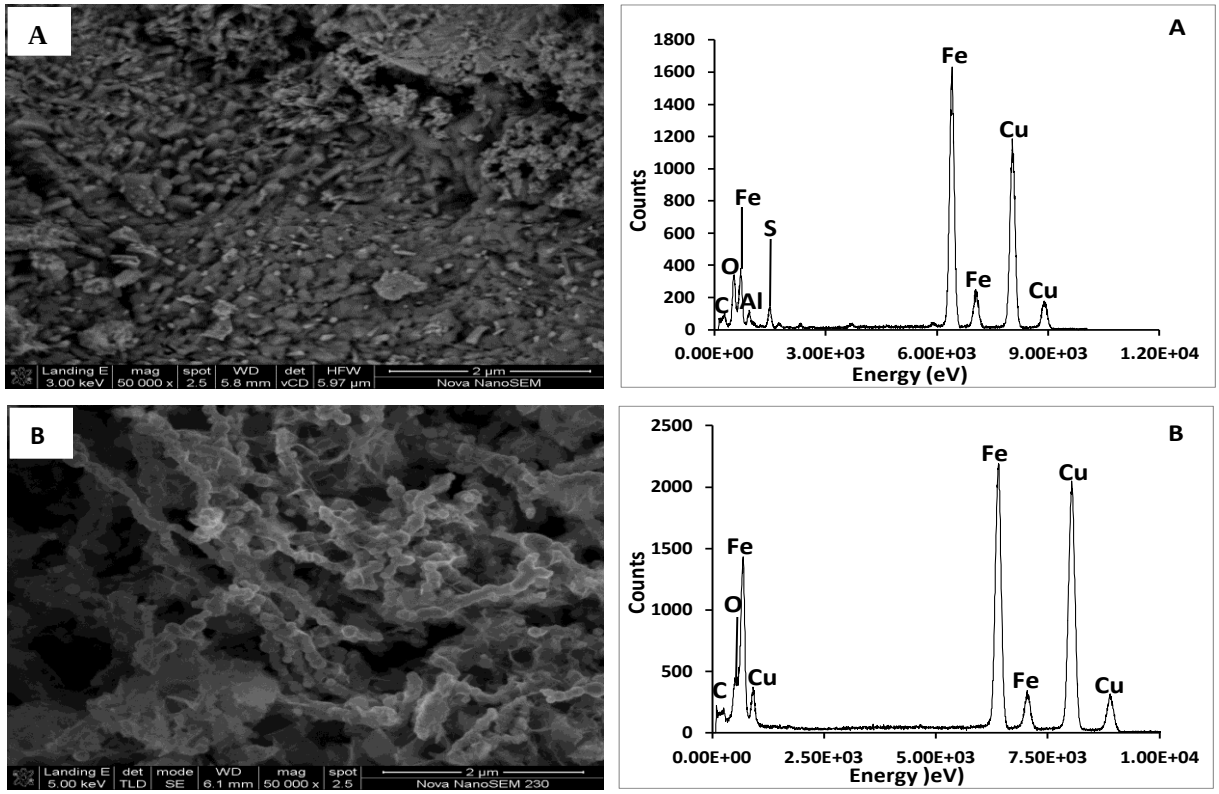

Figure 3. SEM-EDS image and spetral analysis of synthesized iron nanoparticles HAI (A) and HFCI (B). Experimental condition: pH = 2.14 and 1.63, temp = 70℃, speed = 250 rpm, vol. of AMD = 100 mL, vol. of N_2H_4 = 50 mL, Conc. of N_2H_4 = 0.9 M, time = 60 mins and n = 3, HAI = Hydrazine AMD synthesized iron, HFCI = Hydrazine ferric chloride synthesized iron

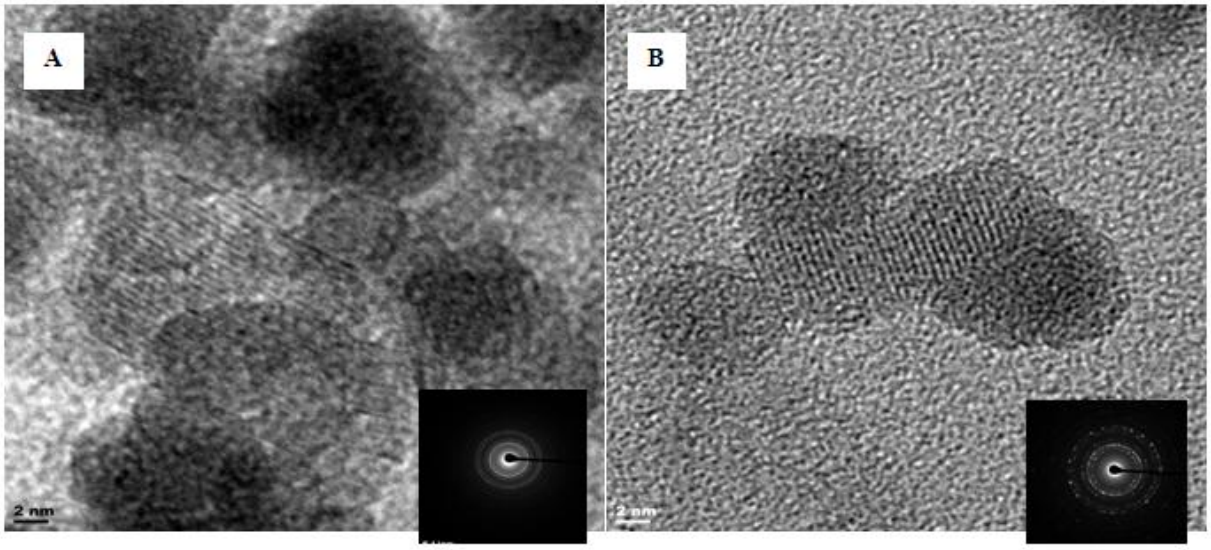

Figure 4. HRTEM-SAED morphology of iron nanoparticles HAI (A) and HFCI (B). Experimental conditions: pH = 2.14 and 1.63, temp = 70℃, speed = 250 rpm, vol. of AMD = 100 mL, vol. of N_2H_4 = 50 mL, Conc. of N_2H_4 = 0.9 M, time = 60 mins and n = 3, HAI = Hydrazine AMD synthesized iron, HFCI = Hydrazine ferric chloride synthesized iron

3.5. XRF

The XRF elemental composition of the synthesized iron nanoparticles HAI and HFCI presented in Table 2 shows the chemical composition of the two synthesized iron samples HAI and HFCI are majorly composed of pure iron (Fe) particles with about 96.7 ± 0.36% and 98.1 ± 0.8% respectively. HAI contained other elements like Al, Si, Ca and S which can be attributed to the source of the iron salt solution while HFCI is free from these contaminants due to the purity of the iron salt from contaminant.

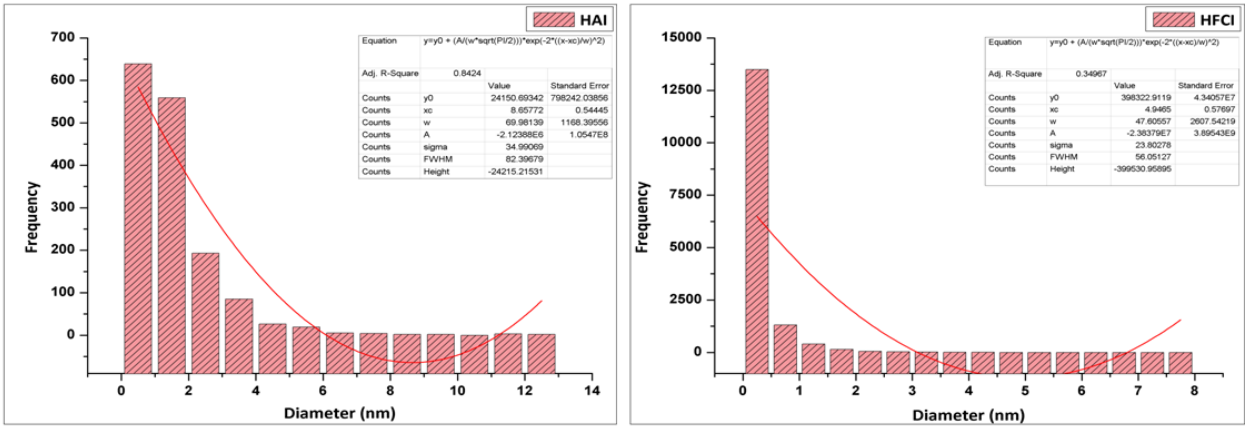

Figure 5. Histogram of crystal size distribution of synthesized iron nanoparticles HAI (A) and HFCI (B). Experimental conditions: pH = 2.14 or 1.63, temp = 70℃, speed = 250 rpm, vol. of AMD = 100 mL, vol. of N_2H_4 = 50 mL, Conc. of N_2H_4 = 0.9 M, time = 60 mins and n = 3, HAI = Hydrazine AMD synthesized iron, HFCI = Hydrazine ferric chloride synthesized iron

Table 2. XRF elemental composition of HAI and HFCI nanoparticles. Experimental conditions: AMD pH = 2.14, $FeCl_3$ pH = 1.63, temp = 70℃, speed = 250 rpm, vol. of AMD = 100 mL, vol. of N_2H_4 = 50 mL, Conc. of N_2H_4 = 0.9 M, time = 60 mins and n = 3, HAI = Hydrazine AMD iron, HFCI = Hydrazine ferric chloride iron

Elements	Fe	Si	Al	Ca
HFCI	98.07 ± 0.8	ND	0.038 ± 0.01	0.029 ± 0.003
HAI	96.73 ± 0.36	0.10 ± 0.001	1.14 ± 0.02	0.28 ± 0.02

ND Not detected

3.6. BET

The BET surface area of HAI (goethite) and HFCI (magnetite) are 125 ± 3.73 m^2/g and 134 ± 4.24 m^2/g respectively. The surface area for HFCI is similar to some of the one cited in the literature and the value of HAI is very close to that of HFCI. The HAI (goethite) and HFCI (magnetite) shows adsorption isotherm classification to be Type 2 and Type 4 respectively for both particles. The adsorption hysteresis loop indicates they are type H3 for HAI and Type H1 for HFCI with steep and triangular shape (Michal Kruk et al, 2001). 3.4 BET surface area.

The adsorption isotherm shown in Figure 6 for HAI (goethite) and HFCI (magnetite) nanoparticles was Type II and their N_2 adsorption-desorption hysteresis loop classification was H3. The BET surface area for HAI and HFCI particles are 125 ± 3.73 m^2/g and 134 ± 4.24 m^2/g respectively. The value obtained for HFCI was a bit higher than the HAI and this can be due to the fact that chemical reagent used for the synthesis of HFCI was unadulterated while the wastewater from the mine used for the synthesis of HAI contained several inorganic substances. Both iron nanoparticles synthesized from AMD (HAI) and ferric chloride salt (HFCI) had large surface area which is an indication of a good adsorbent suitable for adsorption study. The BET surface area results obtained for HAI and HFCI were higher than some values reported in the literature [37], [31] but lower than the BET of some other iron nanoparticles previously reported in the literature [38], [39]. The synthesized iron nanoparticles from AMD using hydrazine had higher surface area than some made from pure chemicals [40], [41].

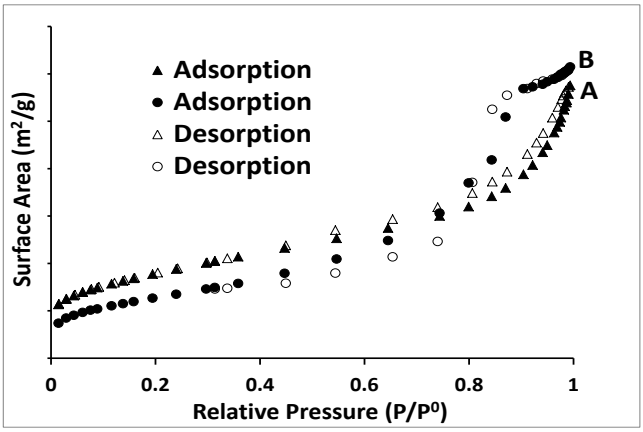

Figure 6. BET adsorption-desorption hysteresis loop of synthesized iron nanoparticles HAI (A) and HFCI (B). Experimental conditions: pH = 2.14, $FeCl_3$ pH = 1.63, temp = 70℃, speed = 250 rpm, vol. of AMD = 100 mL, vol. of N_2H_4 = 50 mL, Conc. of N_2H_4 = 0.9 M, time = 60 mins and n = 3, HAI = Hydrazine AMD synthesized iron, HFCI = Hydrazine ferric chloride synthesized iron

Table 3. BET surface area of synthesized iron nanoparticles HAI (A) and HFCI (B). Experimental conditions: AMD pH = 2.14, $FeCl_3$ pH = 1.63, temp = 70℃, speed = 250 rpm, vol. of AMD = 100 mL, vol. of N_2H_4 = 50 mL, Conc. of N_2H_4 = 0.9 M, time = 60 mins and n = 3, HAI = Hydrazine AMD synthesized iron, HFCI = Hydrazine ferric chloride synthesized iron

Sample	Material Source	Bet Surface Area (m^2/g)
HAI	N_2H_4 and AMD	125 ± 3.73
HFCI	N_2H_4 and ferric chloride	134 ± 4.24

3.7. FTIR

The FTIR absorption spectra of synthesized iron nanoparticles HAI and HFCI are presented in Figure 7. The absorption spectra shows that HAI had peaks at 589 cm^{-1} and 699 cm^{-1}, and the spectra of HFCI at 540 cm^{-1} and 699 cm^{-1} corresponds to Fe-O absorption peaks [42]. The HFCI absorption had a distinct peak at 540 cm^{-1} while the HAI showed a sharp short peak found at 1106 cm^{-1}. [42] reported that the bands of iron nanoparticles around 540 and 699 cm^{-1} corresponded to the bending and stretching vibrations of

Fe-O bonds that are characteristic to the crystalline lattice of magnetite mineral phase. The HAI nanoparticles showed broad absorption stretching bands of O-H stretching at 3263 cm^{-1} which is due to the presence of O-H in the water or alcohol used in rinsing the particles [43]. The O-H bending absorption band at 1653 cm^{-1} and 1518 cm^{-1} of HAI and HFCI nanoparticles confirmed the traces of water [44]. The C-O stretching absorption bands at 1106 and 1120 cm^{-1} confirmed the presence of O-H in the nanoparticles which could be as a result of the presence of water and ethanol used before drying. Only HAI nanoparticles showed a C=O absorption stretching band at (2165-2018 cm^{-1}), which means that HAI particles have strong affinity for CO_2 gas [45], [29]. Synthesis of iron nanoparticles from AMD using hydrazine formed goethite, identified with XRD as a non-magnetic particle with a trace of pure iron (α-Fe) while the synthesis of iron nanoparticles with commercial ferric chloride using hydrazine magnetite is a pure magnetic iron nanoparticle.

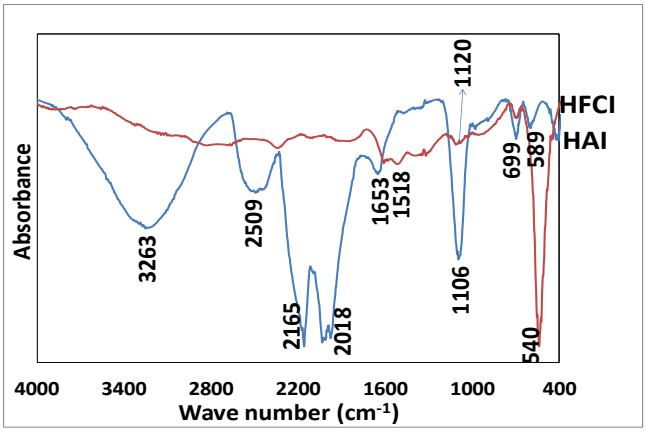

Figure 7. FTIR absorption peaks of synthesized iron nanoparticles HAI (A) and HFCI (B). Experimental conditions: AMD pH = 2.14, $FeCl_3$ pH = 1.63, temp = 70°C, speed = 250 rpm, vol. of AMD = 100 mL, vol. of N_2H_4 = 50 mL, Conc. of N_2H_4 = 0.9 M, time = 60 mins and n = 3, HAI = Hydrazine AMD synthesized iron, HFCI = Hydrazine ferric chloride synthesized iron

4. Conclusions

Iron-rich acid mine drainage (AMD) is an environmental problem used as a substitute to commercial reagent grade iron salt for synthesizing iron nanoparticle. The mine water was used as a cheap feedstock for synthesizing iron nanoparticle in order to save cost of purchasing expensive commercial reagent grade iron salt. The quality of iron nanoparticles synthesized from mine water was characterized using some analytical techniques and XRD identifies goethite mineral phase for AMD (HAI) and magnetite mineral phase for reagent grade (HFCI) source; both particles have large surface area, spherical morphology, and their particle sizes range within 124-135 nm. Fe-O stretching and bending for HAI and HFCI nanoparticles were observed at 699 cm^{-1} and 540 cm^{-1} respectively, while a broad band O—H at 3246 cm^{-1} was observed for HAI. In conclusion, iron-rich AMD is a very good substitute material for commercial reagent grade salts for synthesizing iron nanoparticles.

ACKNOWLEDGEMENTS

I acknowledge the meaningful contributions of the following people to this research work: Water Research Commission (WRC) South Africa, Mrs Ilse Wells, University of The Western Cape (UWC), South Africa, Dr Remy Bucker National Research Fund (NRF) Ithemba-labs, South Africa, and Mrs Miranda Waldron, University of Cape Town (UCT), South Africa.

REFERENCES

[1] Guo, X., & Huang, L. (2012). Recent advances in nonviral vectors for gene delivery. Accounts of chemical research, 45(7), 971-979.

[2] Stark, W. J., Stoessel, P. R., Wohlleben, W., & Hafner, A. J. C. S. R. (2015). Industrial applications of nanoparticles. Chemical Society Reviews, 44(16), 5793-5805.

[3] Bhaumik, A., Samanta, S., & Mal, N. K. (2005). Iron oxide nanoparticles stabilized inside highly ordered mesoporous silica. Pramana, 65(5), 855-862.

[4] Li, Y., and Zhang, F. (2010). Catalytic oxidation of methyl orange by an amorphous FeOOH catalyst developed from a high iron-containing fly ash. Chem Eng J, 158(2), 148-153.

[5] Babay S, Mhiri T, Toumi M (2015). Synthesis, structural and spectroscopic characterizations of maghemite γ-Fe2O3 prepared by one-step coprecipitation route. Journal of Molecular Structure. Volume 1085, 5 April 2015, Pages 286-293.

[6] Nurmi, J. T., Tratnyek, P. G., Sarathy, V., Baer, D. R., amonette, J. E., Specher, K., Wang, C., Linenhan, J. C., Matson, D. W., Leepenn, R., and Driessen, M. D. (2005). Characterization and properties of metallic iron nanoparticles: Spectroscopy, electrochemistry and kinetics. Environ.Sci. Technol, 39, 1221-1230.

[7] Xiao-qin Li, Daniel W. Elliott, and Wei-xian Zhang (2006). Zero-Valent Iron Nanoparticles for Abatement of Environmental Pollutants: Materials and Engineering Aspects. Critical Reviews in Solid State and Materials Sciences, 31: 111–122, 2006.

[8] Shavel, A., Rodríguez-González, B., Spasova, M., Farle, M., & Liz-Marzán, L. M. (2007). Synthesis and characterization of iron/iron oxide core/shell nanocubes. Advanced functional materials, 17(18), 3870-3876.

[9] Setman, D., Schafler, E., Korznikova, E., and Zehetbauer, M. J. (2008). The presence and nature of vacancy type defects in nanometals detained by severe plastic deformation. Materials Science and Engineering: A, 493(1), 116-122.

[10] Ghorbani, H.R., Safekordi, A.A., Attar, H., Rezayat Sorkhabadi, S.M., 2011. Biological and non-biological methods for silver nanoparticles synthesis. Chem. Biochem. Eng. Q. 25 (3), 317–326.

[11] Crane, R., and Scott, T. (2012). Nanoscale zero-valent iron: Future prospects for an emerging water treatment technology. Journal of Hazardous Materials, 211, 112-125.

[12] Mukherjee, J., & Gupta, M. N. (2016). Lipase coated clusters of iron oxide nanoparticles for biodiesel synthesis in a solvent free medium. Bioresource technology, 209, 166-171.

[13] Firestone, M., Kavlock, R., Zenick, H., Kramer, M., & the US EPA Working Group on the Future of Toxicity Testing. (2010). The US Environmental Protection Agency strategic plan for evaluating the toxicity of chemicals. Journal of Toxicology and Environmental Health, Part B, 13(2-4), 139-162.

[14] Alegbe, M. J., Ayanda, O. S., Ndungu, P., Nechaev, A., Fatoba, O. O., & Petrik, L. F. (2019). Physicochemical characteristics of acid mine drainage, simultaneous remediation and use as feedstock for value added products. Journal of Environmental Chemical Engineering, 7(3), 103097.

[15] Mohapatra, M., and Anand, S. (2010). Synthesis and applications of nano-structured iron oxides/hydroxides–a review. International Journal of Engineering, Science and Technology, 2(8).

[16] Cheng, J., Ma, R., Chen, X., Shi, D., Liu, F., and Zhang, X. (2011a). Effect of ferric ions on the morphology and size of magnetite nanocrystals synthesized by ultrasonic irradiation. Crystal Research and Technology, 46(7), 723-730.

[17] Ge, Y., Zhang, Y., Xia, J., Ma, M., He, S., Nie, F., & Gu, N. (2009). Effect of surface charge and agglomerate degree of magnetic iron oxide nanoparticles on KB cellular uptake in vitro. Colloids and Surfaces B: Biointerfaces, 73(2), 294-301.

[18] Wang, M., Wang, C., Wang, G., Zhang, W., & Bin, F. (2010). Synthesis of MnO2/MWNTs nanocomposites using a sonochemical method and application for hydrazine detection. Electroanalysis: An International Journal Devoted to Fundamental and Practical Aspects of Electroanalysis, 22(10), 1123-1129.

[19] Zou, J., Peng, Y. G., & Tang, Y. Y. (2014). A facile bi-phase synthesis of Fe 3 O 4@ SiO 2 core–shell nanoparticles with tunable film thicknesses. RSC Advances, 4(19), 9693-9700.

[20] Laurent S, Forge D, Port M, Roch A, Robic C, Vander Elst L and Muller R N (2008). Magnetic Iron Oxide Nanoparticles: Synthesis, Stabilization, Vectorization, Physicochemical Characterizations, and Biological Applications Chemical Reviews 108 2064-110.

[21] Maiti, D., Manju, U., Velaga, S., & Devi, P. S. (2013). Phase evolution and growth of iron oxide nanoparticles: effect of hydrazine addition during sonication. Crystal growth & design, 13(8), 3637-3644.

[22] Cheng, J., Ma, R., Shi, D., Liu, F., and Zhang, X. (2011b). Rapid growth of magnetite nanoplates by ultrasonic irradiation at low temperature. Ultrasonics sonochemistry, 18(5), 1038-1042.

[23] Cheng, S., Jang, J.-H., Dempsey, B. A., and Logan, B. E. (2011c). Efficient recovery of nanosized iron oxide particles from synthetic acid-mine drainage (AMD) water using fuel cell technologies. Water Research, 45, 303-307.

[24] Dong, Y., Yang, Z., Sheng, Q., & Zheng, J. (2018). Solvothermal synthesis of Ag@ Fe3O4 nanosphere and its application as hydrazine sensor. Colloids and Surfaces A: Physicochemical and Engineering Aspects, 538, 371-377.

[25] Basavaraja, S., Balaji, D. S., Bedre, M. D., Raghunandan, D., Swamy, P. P., & Venkataraman, A. (2011). Solvothermal synthesis and characterization of acicular α-Fe2O3 nanoparticles. Bulletin of materials science, 34(7), 1313-1317.

[26] Lu, L., Ai, Z., Li, J., Zheng, Z., Li, Q., and Zhang, L. (2007). Synthesis and Characterization of Fe-Fe2O3 Core-Shell Nanowires and Nanonecklaces. crystal growth and design, 7.

[27] Andersen, S. L. F., Cardoso, B. P., Flores, R. G., Barbosa, P. R. M., Madeira, V. S., José, H. J., and Moreira, R. F. P. M. (2011). Preparation and characterization of catalysts produced from AMD and their catalytic behavior during toluene oxidation. The International Conference on Environmental Pollution and Public Health (EPPH 2011), 10(12), 1-4.

[28] Flores, R. G., Andersen, S. L. F., Maia, L. K. K., José, H. J., and Moreira, R. d. F. P. M. (2012). Recovery of iron oxides from acid mine drainage and their application as adsorbent or catalyst. Journal of Environmental Management, 111, 53-60.

[29] Ghosh, M. K., Poinern, G. E. J., Issa, T. B., and Singh, P. (2012). Arsenic adsorption on goethite nanoparticles produced through hydrazine sulfate assisted synthesis method. Korean Journal of Chemical Engineering, 29(1), 95-102.

[30] Li, T., Li, S., Wang, S., An, Y., and Jin, Z. (2009). Preparation of Nanoiron by Water-in-Oil (W/O) Microemulsion for Reduction of Nitrate in Groundwater. J. Water Resource and Protection, 1, 1-57.

[31] Yuvakkumar, R., Elango, V., Rajendran, V., and Kannan, N. (2011). Preparation and characterization of zero valent iron nanoparticles. Digest Journal of Nanomaterials and Biostructures, 6(4, October-December), 1771-1776.

[32] Kazemzadeh, H., Ataie, A., and Rashchi, F. (2012). Synthesis of magnetite nano-particles by reverse co-precipitation. International journal of modern physics: conference series, 5, 160-167.

[33] Russo, P., Acierno, D., Palomba, M., Carotenuto, G., Rosa, R., Rizzuti, A., and Leonelli, C. (2012). Ultrafine magnetite nanopowder: Synthesis, characterization, and preliminary use as filler of polymethylmethacrylate nanocomposites. Journal of Nanotechnology, 2012.

[34] Hwang, S. W., Umar, A., Dar, G. N., Kim, S. H., & Badran, R. I. (2014). Synthesis and characterization of iron oxide nanoparticles for phenyl hydrazine sensor applications. Sensor Letters, 12(1), 97-101.

[35] Wang, Q., Kanel, S. R., Park, H., Ryu, A., and Choi, H. (2009). Controllable synthesis, characterization, and magnetic properties of nanoscale zerovalent iron with specific high Brunauer–Emmett–Teller surface area. Received: J Nanopart Res 11, 749-755.

[36] Ou, P., Xu, G., Ren, Z., Hou, X., and Han, G. (2008). Hydrothermal synthesis and characterization of uniform α-FeOOH nanowires in high yield. Materials Letters, 62(6), 914-917.

[37] Celebi, O., Üzüm, Ç., Shahwan, T., and Erten, H. (2007). A radiotracer study of the adsorption behavior of aqueous Ba2+ ions on nanoparticles of zero-valent iron. Journal of

Hazardous Materials, 148(3), 761-767.

[38] Karatapanis, A. E., Petrakis, D. E., and Stalikas, C. D. (2012). A layered magnetic iron/iron oxide nanoscavenger for the analytical enrichment of ng-L< sup>− 1</sup> concentration levels of heavy metals from water. Analytica chimica acta, 726, 22-27.

[39] Giraldo, L., and Moreno, J. C. (2013). Synthesis of magnetite nanoparticles and exploring of application in the removal of ions Pt2+ and Au3+ from aqueous solutions. European Chemical Bulletin, 2(7), 445-452.

[40] Kanel, S., Greneche, J., and Choi, H. (2006). Arsenic (V) removal from groundwater using nanoscale zero valent iron as a colloidal reactive barrier material. Environ. Sci. Technol., 40, 2045-2050.

[41] Wang, G., Gou, X., Horvat, J., and Park, J. (2008). Facile synthesis and characterization of iron oxide semiconductor nanowires for gas sensing application. The Journal of Physical Chemistry C, 112(39), 15220-15225.

[42] Roonasi, P. (2007). Adsorption and surface reaction properties of synthesized magnetite nanoparticles. Division of chemistry department of chemical engineering and geosciences, Lulea University of Technology S-971 87 Lulea, Sweden.

[43] Cai, W., and Wan, J. (2007). Facile synthesis of superparamagnetic magnetite nanoparticles in liquid polyols. Journal of Colloid and Interface Science, 305(2), 366-370.

[44] Duhan, S., and Devi, S. (2010). Synthesis and structural characterization of iron oxide-silica nanocomposites prepared by the sol gel method. Int. J. Electr. Eng, 2, 89-92.

[45] Li, X.-q., and Zhang, W.-x. (2007). Sequestration of Metal Cations with Zerovalent Iron Nanoparticles, A Study with High Resolution X-ray Photoelectron Spectroscopy (HR-XPS). J. Phys. Chem. C 111, 6939-6946.

Copyright © 2022 The Author(s). Published by Scientific & Academic Publishing
This work is licensed under the Creative Commons Attribution International License (CC BY). http://creativecommons.org/licenses/by/4.0/